



ISSN: 0067-2904

## Structural, Gas Sensing and Dielectric Properties of $\text{Ho}_x\text{Fe}_{1-x}\text{FeO}_3$ Perovskite Compound

Ali Abd Al- Aleem\*, Muthafar F. Al-Hilli

Department of physics, college of science, university of Baghdad, Baghdad, Iraq

Received: 26/10/2021

Accepted: 9/1/2022

Published: 30/8/2022

### Abstract

Environmental pollutions and resources depletion motivates scientific research to innovate technologies for sustainable productive systems. To develop gas sensing substance with optimized performance a perovskite compound of  $\text{Ho}_x\text{Fe}_{1-x}\text{FeO}_3$  (where  $x= 0, 0.01, 0.03$  and  $0.05$ ) were prepared by standard solid state reaction technique. The crystal structure was studied by XRD, which confirmed the formation of polycrystalline orthorhombic structure with space group Pbnm type perovskite. The preferred crystal growth of the main peak was (211). The structural parameters were also calculated and it was found that the lattice constants and particle size increased with the Ho doping ratio. The electrical properties were studied using the Hall effect, studied using the Hall effect, where the Hall coefficient, D.C conductivity (from  $2.24\text{E}-06$  ( $\Omega^{-1}.\text{cm}^{-1}$ ) at  $x=0$ ) to  $2.67\text{E}.$   $-06$  ( $\Omega^{-1}.\text{cm}^{-1}$ ) at  $x=0.05$ ), mobility)  $7.26$  ( $\text{cm}^2 / \text{V}.\text{sec}$ ) at  $x=0$  and decreased to  $5.97$  ( $\text{cm}^2 / \text{V}.\text{sec}$ ) at  $x=0.05$ ) and the concentration of charge carriers ( $2.14 \text{E}13 \text{ cm}^{-3}$  at  $x=0$ ) to  $2.79\text{E}.$   $13 \text{ cm}^{-3}$  at  $x=0.05$ ) were calculated. The charge carrier concentration increased and charge mobility decreased with Ho addition. The Hall coefficient results revealed an n-type conduction mechanism. The dielectric constant  $\epsilon_r$  (in its real and imaginary parts) decreased with the increase in frequency of the applied electric field.  $\tan \delta$  and the AC conductivity were also calculated, and It was found that with the raise in the doping rate, the values of AC conductivity increase while  $\tan \delta$  decreases.

**Keywords:** orthorhombic, perovskite, Hall effect, dielectrics, bulk gas sensors.

### الخواص التركيبية والتحسسية للغاز والعزلية لمركب بيروفسكايت $\text{Ho}_x\text{Fe}_{1-x}\text{O}_3$

علي عبد العليم\*, مظفر فؤاد الحلي

قسم الفيزياء, كلية العلوم, جامعة بغداد, بغداد, العراق

#### الخلاصة

حفزت مشاكل تلوث البيئة البحث العلمي نحو ابتكار تقنيات تقوم باستشعار وجود ونسبة الغازات، تم تحضير مركب بيروفسكايت  $\text{Ho}_x\text{Fe}_{1-x}\text{O}_3$  بتراكيز مختلفة بواسطة تقنية تفاعل الحالة الصلبة القياسية. تمت دراسة التركيب البلوري بواسطة XRD، والذي أكد تكوين تركيب هيكل معيني متعدد التبلور له مجموعة فضاء Pbnm، كما وجد أن ثوابت الشبكة وحجم الجسيمات يزدادان مع زيادة نسبة التشويب. كما تم دراسة الخواص الكهربائية باستخدام تأثير هول حيث كشفت النتائج أن لها خصائص شبه موصلة، كما ظهر أنه مع زيادة

\*Email: [ezzaldeenbaghdady@yahoo.com](mailto:ezzaldeenbaghdady@yahoo.com)

التشويب فإن تركيز حاملات الشحنة يزداد. كما ظهر من خلال جهاز LRC meter انخفاض ثابت العزل (الحقيقي والخيالي) وقيم  $\tan \delta$  وازدياد موصلية التيار المتناوب مع زيادة تردد المجال الكهربائي المطبق. كما تبين أن المركب له خصائص حساسية جيدة لغاز  $\text{NH}_3$ .

## Introduction

Recently, the importance of sensors has increased, especially bulk gas sensors, or what is sometimes expressed as "the electronic nose" in addition to those of semiconducting materials made of metal oxides, because of their durability, abundance of practical applications and cheapness[1]. Metal oxides have many applications, as semiconductor metal oxide sensors are used in many fields in industry, including measuring the quantities of gases polluting the environment. The charge carriers concentrations on the semiconductor surface change according to the compounds of the surrounding atmosphere; the interaction of a target gas with a sample of metal oxides leads to a change in the concentration of charge carriers, which leads to a change in conductivity or resistance [2].

The study of the Hall effect is a standard tool for studying the mobility and type of charges in materials by measuring the Hall potential difference  $V_H$  and Hall coefficient, as shown in the following equation[3]:

$$R_H = \frac{1}{nq} \quad \dots\dots\dots (1)$$

Where: n is the concentration of charge carriers and q is the charge of electron. The  $R_H$  sign in Equation (1) is positive for a p-type semiconductor while it is negative for an n-type.

The concentration of charge carriers n can be calculated by the equations [4]:

$$n = \frac{-1}{R_H q} \quad \text{when} \quad n \gg p \quad \dots\dots\dots (2-a)$$

$$n = \frac{1}{R_H q} \quad \text{when} \quad p \gg n \quad \dots\dots\dots (2-b)$$

The Hall mobility is equal to the product of the Hall coefficient  $R_H$  and the conductivity:

$$\mu = \frac{\sigma}{ne} = \sigma |R_H| \quad \dots\dots\dots (3)$$

Where:  $\sigma$  is the conductivity measured in units  $(\Omega \cdot \text{cm})^{-1}$ , e is the electron charge and  $R_H$  is the conductivity measured in units  $(\text{cm}^2/\text{V.s})$ .

Permittivity determines the response of an insulating medium to an electric field. It is determined by the material's ability to be polarized in response to the electric field. It thus reduces the electric field inside the material, so an increased amount of energy can be stored in a capacitor by placing a high permittivity insulator between its plates. The dielectric constant consists of two parts: real  $\epsilon'$  which represents the amount of energy stored when the material is exposed to an alternating electric field, and imaginary  $\epsilon''$  which represents how much energy is absorbed or dissipated into local defects or grain boundaries, under the influence of the alternating electric field[5].

They are given by the following equations:

$$\epsilon' = \frac{Ct}{\epsilon_0 A} \quad \dots\dots\dots (4)$$

$$\epsilon'' = \frac{d}{A\epsilon R\omega} \quad \dots\dots\dots (5)$$

Where: C is the capacity (Farad), d is the thickness of the sample (m), A is the area of the electrodes ( $\text{m}^2$ ),  $\epsilon_0$  is the space permittivity ( $8.85 \times 10^{-12}$ ), f is the frequency (Hz),  $\omega$  is the angular frequency =  $2\pi F$ , and R is the sample's resistance.

When an alternating electric field is applied, energy loss in dielectrics, called dielectric loss, is produced in the material due to the leakage current resulting from a rise in the frequency of the applied electric field or due to the internal friction of the dipoles [6]. The dielectric loss is a measure of the insulating efficiency of a material and it is expressed by the tangent function of the angle  $\delta$  (Equation 6) . It is called the loss angle. It has been experimentally proven that

the phase angle between current and voltage is less than ( $90^\circ$ ) with a small angle called the angle loss, symbolized by ( $\delta$ ).

$$\tan \delta = \frac{\epsilon''}{\epsilon'} \quad \dots\dots\dots (6)$$

As for the AC conductivity, it represents a measure for the lost energy when an external alternating electric field is applied, as a result of friction between dipoles as they rotate in position or due to collision between particles in the material due to a change in the frequency of the alternating electric field [5].

$$\sigma_{AC} = 2 \pi f \epsilon_0 \epsilon' \quad \dots\dots\dots (7)$$

Where:  $t$  is the thickness of the sample (mm),  $C$  is the capacitance value (F),  $A$  is the area of the plates  $\text{mm}^2$ ,  $\epsilon_0$  is the permittivity of the air of  $8.854 \times 10^{-12} \text{ Fm}^{-1}$ ,  $R$  is the resistance (Ohm), and  $f$  is the frequency applied electric field to the sample (Hz).

A sensor is a device that detects a physical condition in a place, such as determining the presence of a particular gas. It converts the signals that fall on it into electrical impulses that can be measured or counted by a device. The sensor, in its simplest form, consists of a gas-sensitive material and an electronic circuit to determine the concentration of the escaping gas.

### Experimental:

After mixing and weighing, 4 samples were formed from  $\text{Ho}_x\text{Fe}_{1-x}\text{FeO}_3$ , where ( $x= 0, 0.01, 0.03, 0.05$ ) by uniaxial pressing in a steel mold with a cavity diameter of 1.5 cm. The blended mixture was placed inside the piston mold carefully. A forming pressure of 2000 Pa was applied for 2 min to each sample, and cylindrical samples with a diameter of 1.45 cm and a thickness of 0.285 cm were obtained. The sintering process was carried out in a (local origin) furnace at a temperature of 1150 °C/min soaking time. Then it was slowly cooled until it reached room temperature room.

X-ray diffraction patterns were obtained using an XRD-6000 device (manufactured by SHIMADZU of Japanese origin, with an inlet voltage of 220) in a range of  $2\theta$  angles between  $20^\circ$  and  $80^\circ$ . The target used in the X-ray tube was Cu  $K\alpha$  with wavelength = 1.54060 Å. The X-ray patterns were used to calculate the lattice parameters from the  $d$ -spacing by the equation for orthorhombic structure [7]:

$$\frac{1}{d^2} = \frac{h^2}{a^2} + \frac{k^2}{b^2} + \frac{l^2}{c^2} \quad \dots\dots\dots (8)$$

where  $h$ ,  $k$  and  $l$  are the miller's indices. The X- ray density was calculated from:

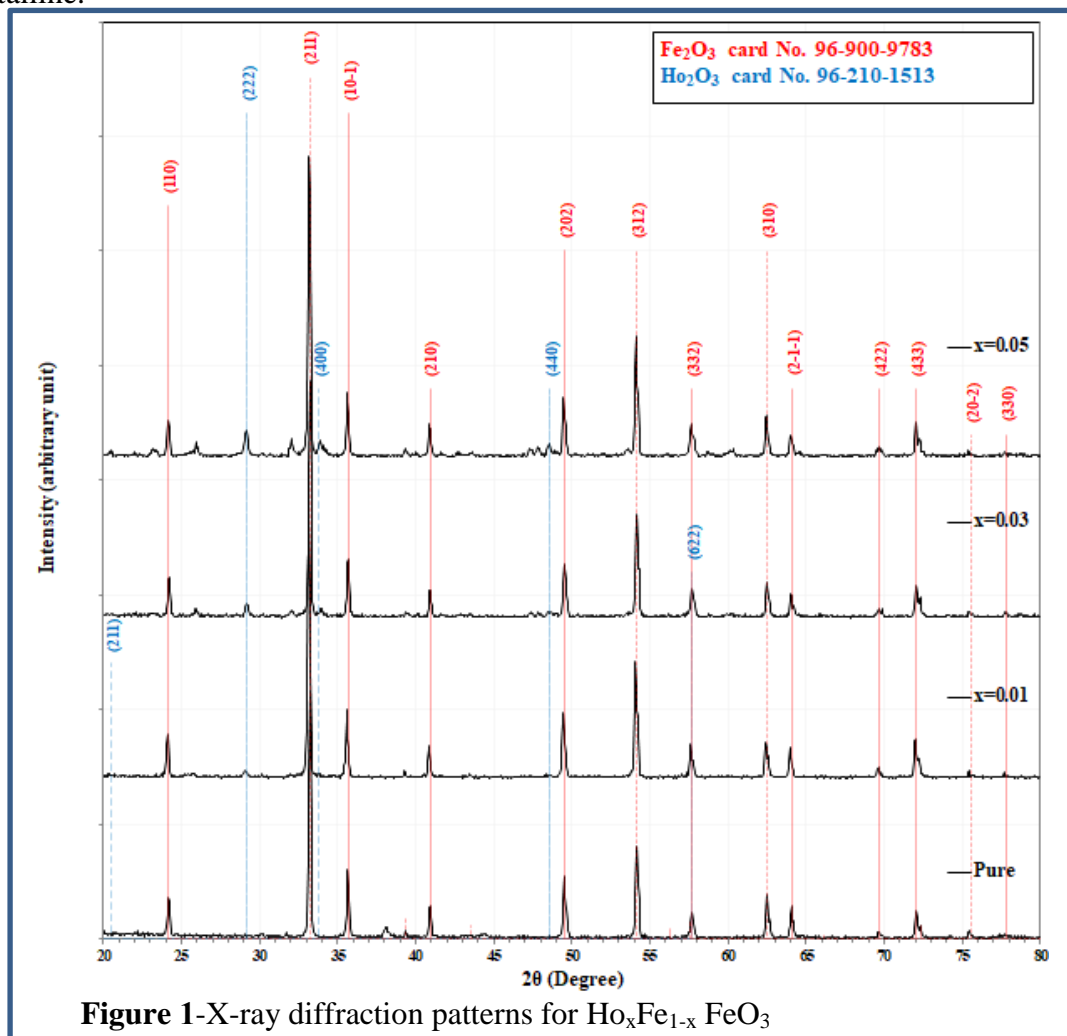
$$d_x = \frac{ZM}{Na^3} \quad \dots\dots\dots (9)$$

Where:  $Z$  is number of molecules per unit cell ( $Z=4$ ),  $M$  is the molecular weight and  $N$  is Avogadro's number ( $N= 6.022 \times 10^{23} / \text{mol}$ ). Hall effect test was carried out using a Kobe Model HMS-5000 device with a density magnetic field of 0.55 Tesla. The aim of the examination was to determine the Hall coefficient, where the sign of the Hall coefficient indicates the type of charge carrier, whether it is negatively charged (electrons) or positively charged (holes). The test also aims to determine the concentration of charge carriers and the mobility value at room temperature. Both sides of the samples were coated with silver paste and two wires were welded with silver paste on both sides of the sample. Dielectric constant (real and imaginary), loss angle  $\tan\delta$  and  $\sigma_{AC}$  in the frequency range (200 kHz - 1 MHz) were obtained. Sensitivity tests for  $\text{NO}_2$  gas were carried out using a homemade system consisting of a stainless steel cylinder as the gas sensing chamber. The sensor system contains a needle valve to control the entry and exit of gas, and it is connected by a tube to a flask containing  $\text{NO}_2$  gas. The system also contains a base on which samples are placed inside the sensing chamber, and a thermal heater to raise the temperature. The sensors were connected to a digital counter (thermometer) (type UNT-TUT81B) to control the operating temperature. Firstly, the resistance of the sample in the air was measured, and then the samples were inserted into a vacuum chamber. The aluminium electrodes deposited on the sample were

connected to wires that fixed the sample on the base inside the sensing chamber; next, the gas was pumped into the vacuum chamber and the change in the resistance of the sample was read every second at a constant temperature.

### Results and discussion:

X-ray diffraction patterns for samples of  $\text{HoFeO}_3$  are shown in Figure 1. The values of the interatomic distances  $d$  for each sample were obtained directly by a computer connected to the device, and were mathematically obtained by applying Bragg's law. The phases formed can be obtained by comparing the values of the interactions  $d$  (between the diffracted levels and the intensity of the diffracted rays) with the standard reference tables ASTM (JCPDS File No. 46-0115) [8]. However, in the present case the phases were obtained using analysis software Match. The X-ray diffraction analysis of  $\text{HoFeO}_3$  indicates that all the samples have an orthorhombic structure with space group  $\text{Pbnm}$ , this agrees with Marezio [9]. Nine peaks appeared in the X-ray diffraction spectrum of  $\text{Ho}_x\text{Fe}_{1-x}\text{FeO}_3$ , which means that the structure is polycrystalline.



One can notice that peak (211) dominates the other peaks, which means that it is the preferred direction for crystal growth. As for  $\text{Ho}_x\text{Fe}_{1-x}\text{FeO}_3$ , the values of  $2\theta$  determined in the case of  $x = 0.01$  were:  $24.1356^\circ$ ,  $29.0909^\circ$ ,  $33.158^\circ$ ,  $35.6038^\circ$ ,  $40.8486^\circ$ ,  $54.0818^\circ$ ,  $57.6334^\circ$ ,  $62.4182^\circ$ ,  $63.9731^\circ$ ,  $69.626$ , and  $72.0062$  and these values corresponds to another value for Miller levels (222), (211), (10-1), (210), (202), (312), (332), (310), (2-1-1), (422), and (433) respectively.

The  $2\theta$  values corresponding to the diffraction peaks were also determined in the case of  $x = 0.05$ , which were:  $24.1786^\circ$ ,  $29.1686^\circ$ ,  $33.1933^\circ$ ,  $33.8828^\circ$ ,  $35.6408^\circ$ ,  $40.8905^\circ$ ,  $48.5289^\circ$ ,  $49.5302^\circ$ ,  $54.1487^\circ$ ,  $57.7061^\circ$ ,  $62.4840^\circ$ ,  $64.0312^\circ$ ,  $69.6622^\circ$ , and  $72.0573^\circ$ . These are referred to (110), (222), (211), (400), (10-1), (210), (440), (202), (312), (332), (310), (2-1-1), (422) and (433) plane direction, respectively. Equations (8) and (9) can be applied to calculate the lattice parameters, which are as shown in Table 1.

**Table 1-** lattice parameters for  $\text{Ho}_x\text{Fe}_{1-x}\text{FeO}_3$

X	M (g/mol)	a Å	b Å	c Å	$V * 10^{-22}$ $\text{cm}^3$	G.S.	FWHM (Deg)	$d_x$ ( $\text{g}/\text{cm}^3$ )	$2\theta$ (Deg)
0.01	104.42	5.278	5.591	7.602	2.243	49.3	0.1683	3.092	33.1580
0.03	105.642	5.284	5.598	7.622	2.255	49.02	0.1642	3.1112	33.2403
0.05	106.866	5.292	5.604	7.648	2.268	48.98	0.1622	3.1296	33.1933

Where:  $x$  is the doping ratio,  $M$  is the molecular weight,  $V$  is the cell volume, G.S is the grain size, and  $d_x$  is the X-ray density. It was found that the lattice parameter increased with the increase of doping; accordingly, the cell size increased. This may be due to the higher ion radius of Ho. It is noted that the higher the doping, the higher the parameters, and the cell size increases accordingly. The structure of  $\text{Ho}_x\text{Fe}_{1-x}\text{FeO}_3$  is not ideal perovskite, and the  $\text{Fe}^{+3}$  ions and  $\text{O}^{2-}$  ions depart from the ideal positions due to the difference between the radius of Ho ions and the Fe ions.

It can be seen that the crystal size decreased with the increase in the proportion of Ho, because the Ho ions prevent grain growth during the sintering process, which leads to a reduction in the crystal size [10].

#### Hall effect measurements:

The results of the Hall effect can be seen in Table 2 using Equations 1,2 and 3.

**Table 2-**lattice parameters and Hall Effect for  $\text{Ho}_x\text{Fe}_{1-x}\text{FeO}_3$

x	$R_H$ ( $\text{cm}^3/\text{C}$ )	$n \times 10^{13}$ ( $\text{cm}^{-3}$ )	$\mu_H$ ( $\text{cm}^2/\text{v}.\text{sec}$ )	$\sigma_{D,C}$ ( $\Omega^{-1}.\text{cm}^{-1}$ )
0	-3.24E+06	1.93	7.26	2.24E-06
0.01	-2.93E+06	2.14	7.02	2.40E-06
0.03	-2.59E+06	2.41	6.73	2.60E-06
0.05	-2.24E+06	2.79	5.97	2.67E-06

Where  $x$  is the doping ratio,  $R_H$  is the Hall coefficient,  $\mu_H$  is mobility, and  $\sigma_{D,C}$  is A.C. conductivity. All samples possessed n-type conductivity mechanism. This may be due to the lack of  $\text{Fe}^{2+}$  ions and the occurring of a vacancy as a result of removing the  $\text{Fe}^{2+}$  ion leave two weakly bonded electrons and therefore this vacancy becomes a double donor. Figure 2 shows a clear increase in the concentration of carrier materials when adding impurities, as it increased from  $1.93 \times 10^{13}$  ( $\text{cm}^{-3}$ ) at  $x=0$  to  $2.79 \times 10^{13}$  ( $\text{cm}^{-3}$ ) at  $x=0.05$ .

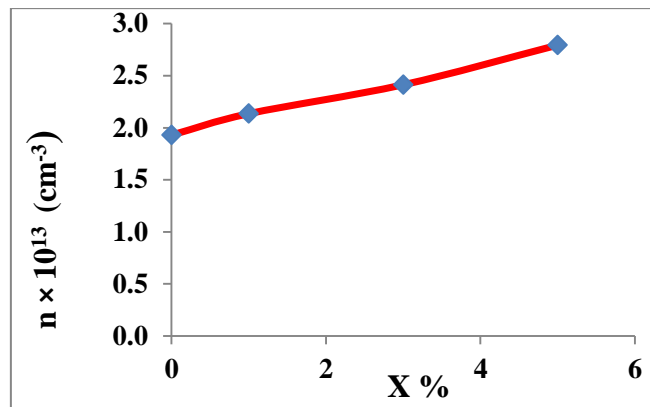


**Figure 2-**Relation between doping and concentration of carriers

The rise in the ratio of charge carriers was due to the increase in the concentration of carriers in the local levels formed near the conduction band, which leads to a rise in the number of electron-donating atoms capable of ionization within non-ionizing thermal energy that does not exceed the value of KBT. The value of mobility was also obtained from the application of Equation (3). As it is clear from Figure 3, the decrease in the mobility values with the increase of doping, where the mobility reached 7.26 (cm<sup>2</sup> / V.sec) at x=0 and decreased to 5.97 (cm<sup>2</sup> / V .sec) at x=0.05. The increase in doping concentration resulted in a decrease in mobility due to the presence of ionized impurities that helps scatter the electrons.

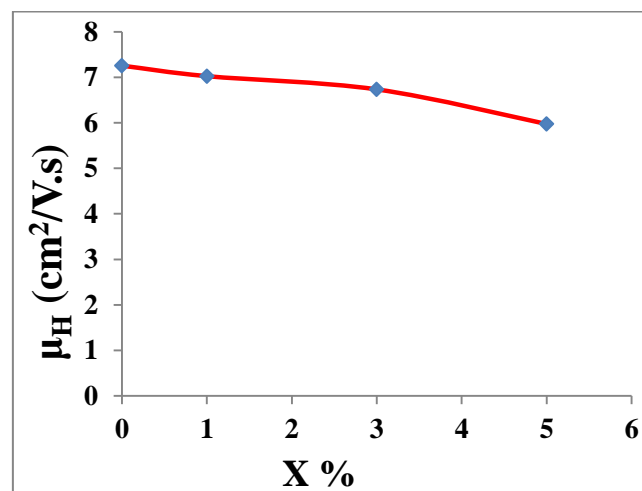


**Figure 3-** Relation between doping and mobility

As for mobility, it can be explained depending on Equation [10]:

$$\mu = \frac{e\tau}{m^*} \tag{9}$$

Where:  $\tau$  is the mean free path time, and  $m^*$  is the effective mass of the electron. An increase in the doping ratio leads to a reduction in the mean free path time, which leads to a slight decrease in the movement value compared to the apparent increase in the concentration of electrons, the latter being responsible for the increase in conductivity at a constant temperature. Figure 4 illustrates the conductivity change with the doping ratio. The electrical conductivity is due, in particular, to exchange of charge carriers between ions in crystalline equivalent positions. It is evident that it increased with the doping ratio from 2.24E-06 ( $\Omega^{-1} \cdot \text{cm}^{-1}$  at x=0 ) to 2.67E-06 ( $\Omega^{-1} \cdot \text{cm}^{-1}$ ) at x=0.05. The increase in conductivity is due to the increase in the charge carriers concentration, as shown in Table 2 [11].

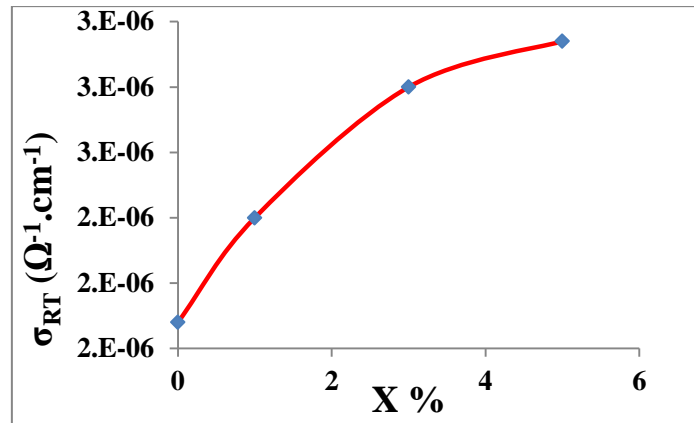


Figure 4-Relation between doping and conductivity.

Figures (5,6,7 and 8) show the results of the dielectric constant (real and imaginary), dielectric loss, angle tangent, and AC conductivity at different electric field frequency for all samples. It is clear from them that the values of the dielectric constant and tan decrease with the increase in the frequency of the electric field, while the values of the AC conductivity increase. This result is in agreement with the results of a number of researchers such as Abdel Rahman [12].

Figure 5 shows the variation of the real part of the dielectric constant with frequency within the range of 200 KHz to 1 MHz, for different doping percentage. A decrease in the values is noticed with increasing the frequency; also an increase in the dielectric constant with the increase in the percentage of doping. The decrease in the value of the dielectric constant with an increase in frequency is because an increase in the frequency of the applied electric field leads to a decrease in the polarity contribution to the total polarization, which leads to a decrease in the values of the dielectric constant [13]. Increasing the frequency also reduces the ability of the induced dipoles to keep up with the change in the electric field, thus reducing the energy they absorb from the applied electric field, which leads to a lower value of the dielectric constant[14].

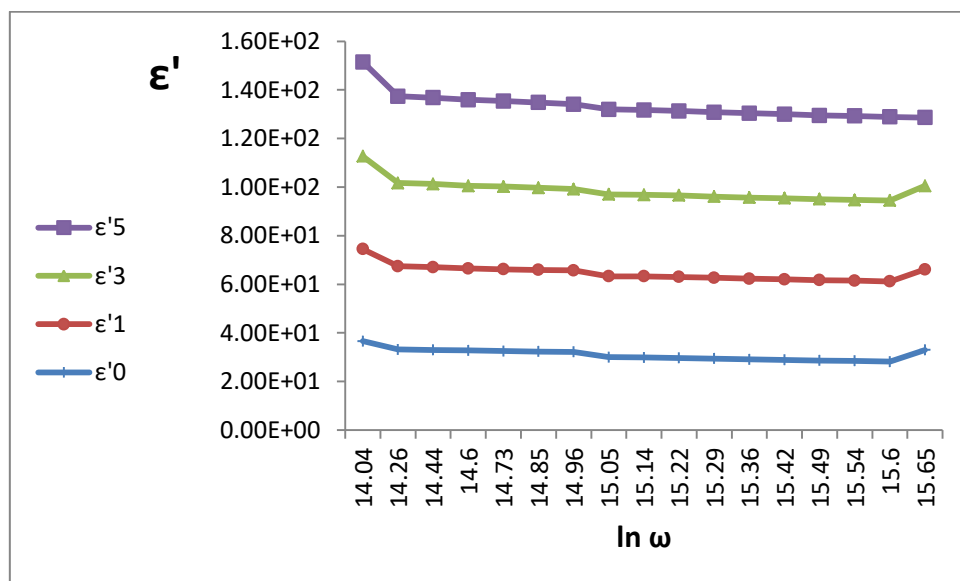
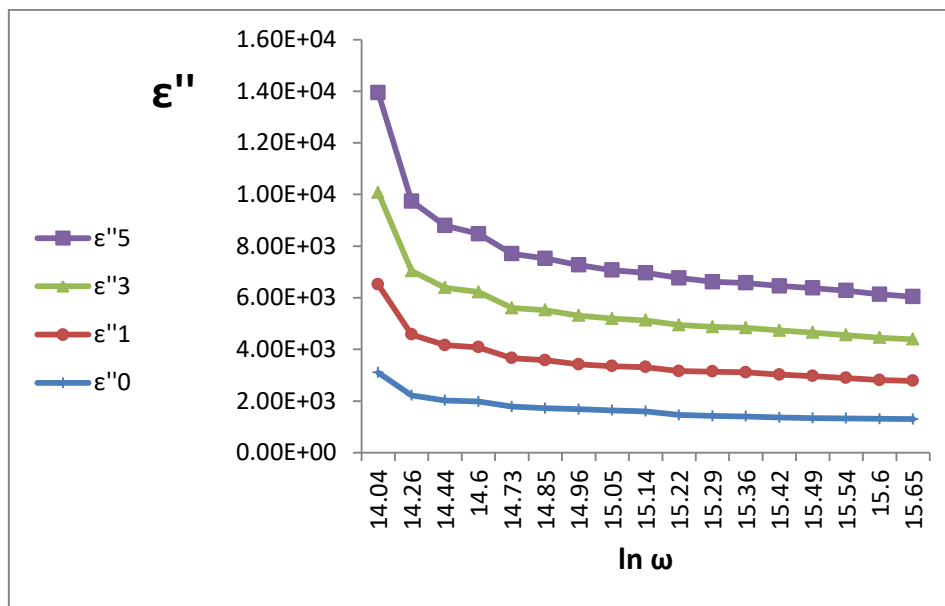


Figure 5- The relationship between dielectric constant and frequency

The doping affects the dielectric properties by hopping of  $Fe^{+2}$  ions exchange reaching to saturated state with impurity ions. This occurs at low frequencies leading to an increase in

dielectric parameters. The dielectric constants starts to decrease with frequency reaching lowest value[15].

As the frequency increases, the value of the imaginary dielectric constant decreases, as shown in Figure 6. The decrease in the values is due to the movement of charge carriers, and also because of their large numbers, through the material, it was possible for their movement to decrease when they meet any phase in the material and because of the multiplicity of phases, the energy absorbed or dispersed decreases. This agrees with Oboudi [16]. As the value of the imaginary dielectric constant decreases, it stabilizes at specific and small values and may reach zero, and this indicates that the imaginary dielectric constant becomes independent, that is, it does not depend on frequency. This case is found in insulators and it is due to the electronic and ionic polarization [17].



**Figure 6-**The relationship between the imaginary part and frequency

It is seen from Figure 7 that the dielectric loss decreases with increasing frequency for all samples. The dielectric loss is caused by thermal irritation and friction impeding the orientation and rotation of the dipoles with the applied electric field [15]. The increase in frequency increases the volumetric and surface leakage current resulting from the presence of impurities and moisture. In addition, the difference in the values of the tangent of the dielectric loss ( $\tan \delta$ ) may be the result of the difference in the distribution of heat on the material in the furnace during the sintering, or due to the inhomogeneity of the distribution of phases inside the compound due to the change in the ratios of substitution and addition [18]. When an external electric field is applied to any material, the waste energy is in the form of heat in insulators or conductors, but in isolation materials the dissipation in power is variable as it depends on the nature of the material and its geometric shape as well as on the frequency of the field.

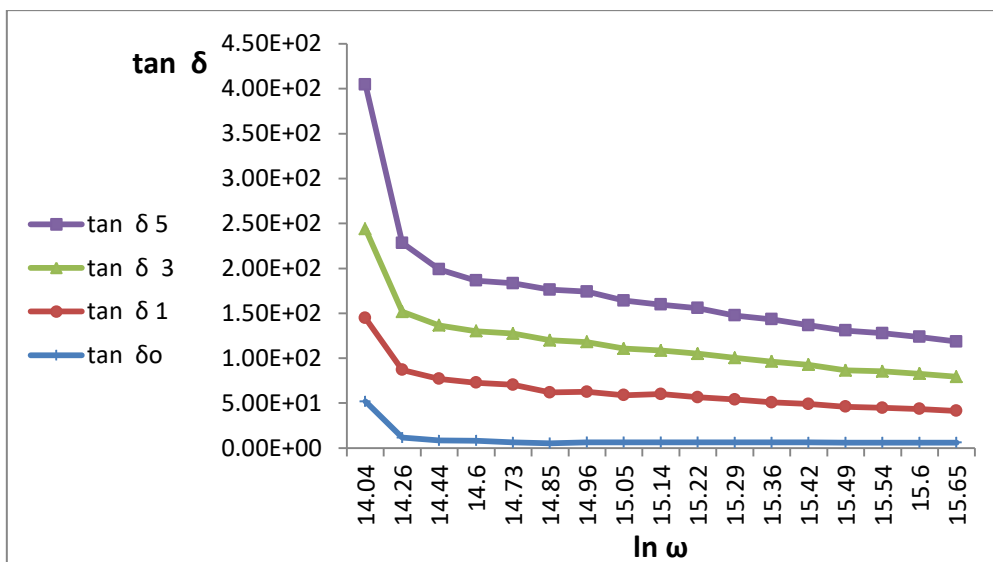


Figure 7- the relationship between the tangent of the angle loss and frequency

As it appears from Figure 8, the AC conductivity is large at high frequency and small at low frequency. The factors that determine the AC conductivity values are the imaginary dielectric constant and the frequency as it is clear from the equation (7), while the rest of the variables are fixed quantities. Frequency has the largest role in the value of the AC conductivity because the value of the imaginary dielectric constant was small with respect to frequency. Thus, when the frequency increases, the mechanical displacement of the ions inside the structure of the phases increases. This leads to an increase in the AC conductivity. Knowing that the values of AC conductivity decrease with the increase in the sintering temperature and time. Higher values of sintering temperature and time lead to an increase in the density and thus a decrease in the porosity, as a result the dissipated energy decreases due to the gaps and defects, and this leads to a reduction in the value of the AC conductivity [19,20].

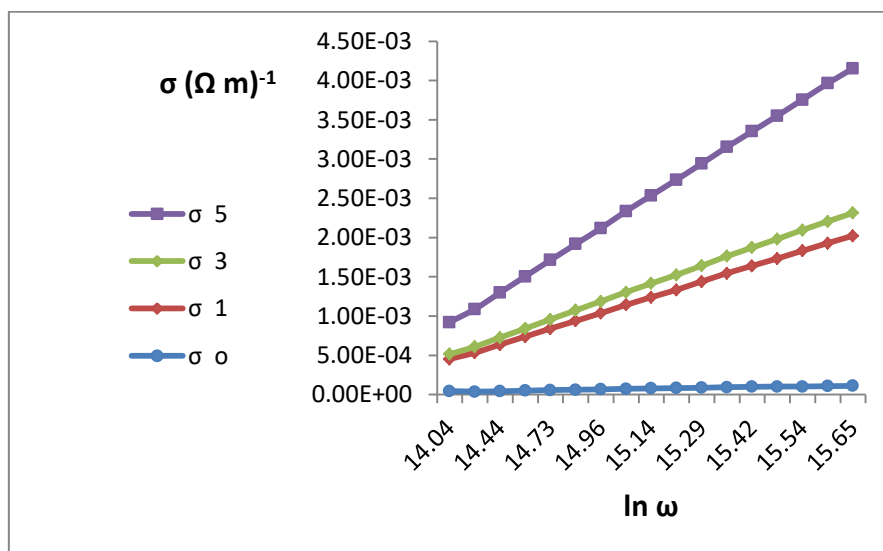
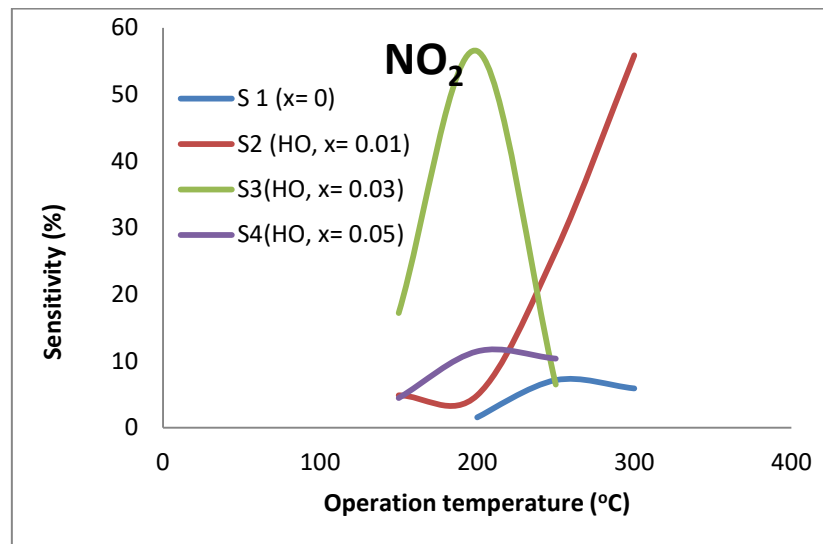


Figure 8-The relationship between AC conductivity and frequency

Figure 9 shows the sensitivity as a function of the operating temperature in the range (25-300 °C) of pure samples Fe<sub>2</sub>O<sub>3</sub> and doped with different concentrations of Ho ions. The sensor test was performed with NO<sub>2</sub> mixed with dry air, where the bias voltage (3V) was applied on the electrodes of all samples.

The change of temperature reveals that the resistance of the samples (sensors) decreases with increasing temperature from room temperature to 300°C, which is an indicative of a typical negative temperature coefficient of resistance (NTCR) due to thermal excitation of charge carriers in semiconductors. But above 300 °C, the sensor displays a Positive Temperature Resistance Coefficient (PTCR), which may be due to saturation of the conduction band with electrons higher than the shallow donor levels caused by oxygen vacancies.

This figure shows the relationship between sensitivity and temperature of a pure and Ho ions doped sensor for NO<sub>2</sub> gas. Ho<sub>x</sub>Fe<sub>1-x</sub> FeO<sub>3</sub> (x= 0.03) sample has the highest sensitivity value for NO<sub>2</sub> gas (56.5%) at a temperature of 200°C. The maximum sensitivity of Ho<sub>x</sub>Fe<sub>1-x</sub> FeO<sub>3</sub> (x= 0.03) gas sensor to 60 ppm of NO<sub>2</sub> was about 56.5% at around 200°C. But the Fe<sub>2</sub>O<sub>3</sub> pure gas sensor had the lowest sensitivity value for NO<sub>2</sub> gas, especially at 200°C where the sensitivity for 60 ppm of NO<sub>2</sub> was 1.57%. It should also be noted that the optimum sensing temperature required for the maximum sensitivity was at around 250°C for Fe<sub>2</sub>O<sub>3</sub> gas sensor. It appeared from all the results that the gas sensitivities to oxidizing gases was significantly improved their performance. Perhaps the reason can be attributed to the size of the Fe<sub>2</sub>O<sub>3</sub> nanoparticle, especially that the grain size is comparable to the depth of the subsurface depletion layers, where the full resistance and sensitivity of the sensor is controlled by the grain itself, implying an inverse relationship between sensitivity and particle size [21].



**Figure 9-** The relation of sensitivity versus operating temperature

The response time was tested for NO<sub>2</sub> oxidizing gas; it increased with the increase of the doping concentration and the operation temperature. The shortest response time was 0.01 sec while it was 11.7 sec at 200 °C for the other samples.

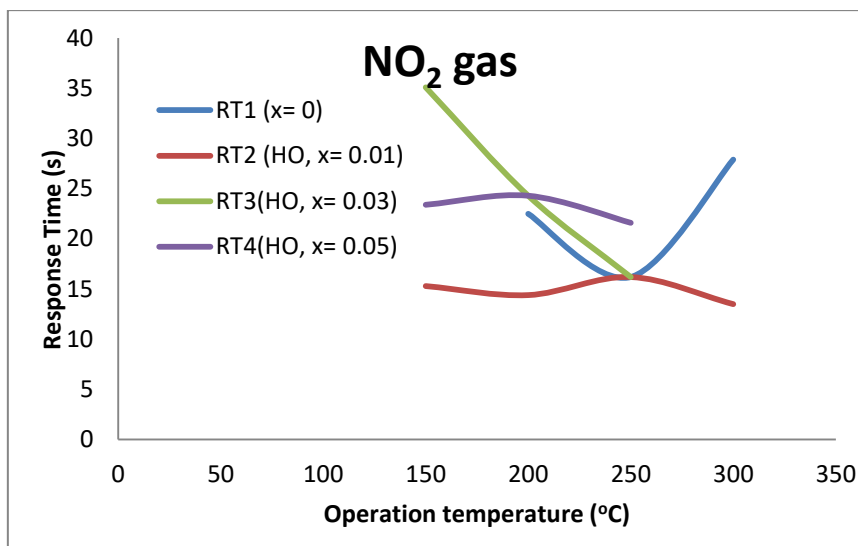


**Figure 10**-Response time versus operating temperature

Figure 1 shows the relationship between the recovery time and the operation temperature for different doping concentrations of the prepared samples. The recovery time decreased with increasing the operation temperature. at a doping concentration of (0.01), the recovery time was 41.4 sec at 200 °C.

The decrease in the doping concentration of the samples (sensors) and the increase in the operating temperature reduced the oxygen adsorption on the surface to obtain the conduction electrons from the near surface region forming the electron depleted surface layer, which resulted in an increase in the number of active adsorption sites and a fast recovery time [22].

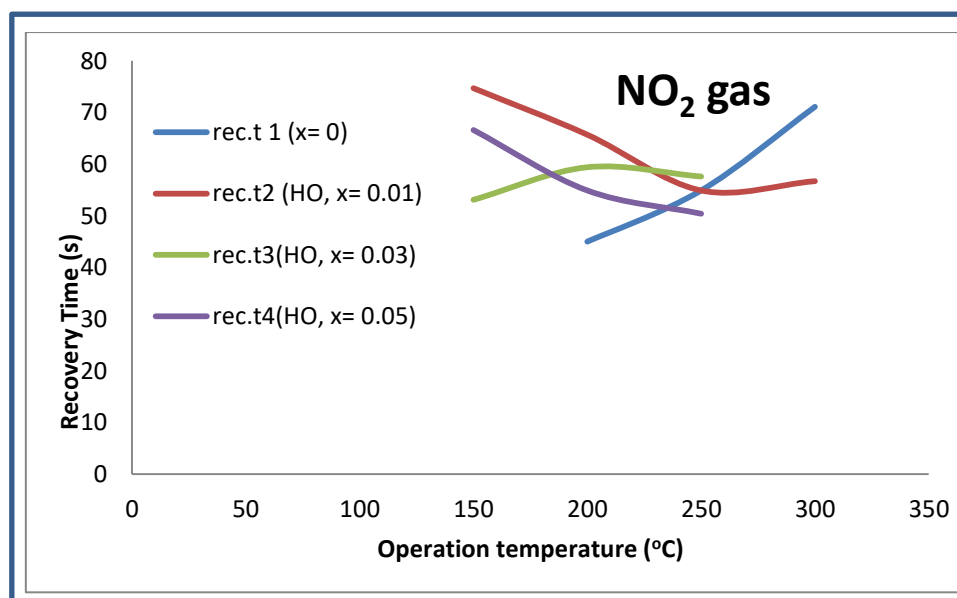


**Figure 11**-Recovery time of the  $\text{Ho}_x\text{Fe}_{1-x}\text{FeO}_3$  gas sensor to the  $\text{NO}_2$  gas as a function of operating temperature.

### Conclusion:

Potentially, perovskites gas sensors to be employed for urbanized ambient quality controlling has drawn much attention in recent years. The high sensitivity results 56.5%; and response time (11.7 s), as well as low recovery time (41.4 s) indicates that this sample has

good sensing properties of NO<sub>2</sub> gas. The ease of manufacturing of Ho<sub>x</sub>Fe<sub>1-x</sub> FeO<sub>3</sub> bulk gas sensor, in addition to its stability and reproducibility makes them promising candidate for developing low-cost sensors.

### References:

- [1] Chan G S., Hsueh T., Chen I., Hsieh S., Change S., Lin Y. and Huang G., 2008- Highly Sensitive ZnO Nanowire Acetone Vapor Sensor With Au Adsorption, *IEEE TRANSACTIONS ON NANOTECHNOLOGY*, p 754-758.
- [2] M. Batzill and U. Diebold- *The surface and materials science of tin oxide - Tulane University, 6400 Freret St., Stern Hall 2001, New Orleans, LA 70118, United States.*
- [3] Daniel D., Harry E. " deposition of Cu In Al Se<sub>2</sub> films" *Apply physics lett*, vol.80, no.7, pp.137-143 , 1997.
- [4] Kittel, Charles - *Introduction to Solid State, 6th addition*, 1956.
- [5] H. Sahi, "Preparation and study the effective of addition In and La) on Bi<sub>2-x</sub>In<sub>x</sub>Sr<sub>2</sub>Ca<sub>2</sub>Cu<sub>3-y</sub>La<sub>y</sub>O<sub>10+δ</sub>) superconductor compound," Ph.D. University of Baghdad college of Education for Pure Science (Ibn Al-Haitham), 2017.
- [6] V.Raghavan, "*Material Science and Engineering*", 5th ed, New Delhi, p 414, 2010
- [7] B. D. Cullity, *Elements of x-ray diffraction*, 2<sup>nd</sup>. edition, 1977.
- [8] M. Marezio, *The Crystal Chemistry of the Rare Earth Orthoferrites* , Bell Telephone Laboratories, Incorporated, Murray Hill, New Jersey, U.S.A. 1969.
- [9] Zubida Habib , M. Ikram , Kowsar Majid and K. Asokan , *Structural, dielectric and ac conductivity properties of Ni-doped HoFeO<sub>3</sub> before and after gamma irradiation*, Springer-Verlag Berlin Heidelberg 2014
- [10] M. M. Elsehly, D. M. Hemeda, and O. M. Hemeda, Phase Transition (Spinel-Ortho) Ferrite Doped with Holmium, *Journal of Applied Mathematics and Physics* , Vol.8 No.4, April 2020
- [11] A. Tribble, "Electrical Engineering Materials and Devices" University of Iowa, (2002).
- [12] Marwa Waleed Abdul Rahman, Preparation of superconducting Y-Ba-Cu-O compounds and study their structural and electrical properties, e College of Education for Pure Science (Ibn AlHaitham), 2019.
- [13] M. Tinkham and C.J. Lobb, " Physical properties of the new superconductors. In Solid State Physics ", In *Solid State Physics*, Vol.42, pp91-134, 1989
- [14] W.B. Michel: "*Fundamentals of Ceramics*", International Editions, The McGraw-Hill companies, Inc. New York. 1997.
- [15] Mukhlis M. Ismail and Nasma A. Jaber , Dielectric properties of Li doped Ni-Zn ferrite Department of Applied Sciences, University of Technology, Baghdad, Iraq, 2018.
- [16] S. F. Oboudi, M. Q. M. AL-Habeeb, "Dielectric and Transport Properties of Ag Nanoparticles added Bi<sub>1.7</sub>Pb<sub>0.3</sub>Sr<sub>2</sub>Ca<sub>2</sub>Cu<sub>3</sub>O<sub>10+δ</sub> Superconductor Compound", *AARJMD*, Vol.3, Issue.3, 2016.
- [17] R. Choudhary, R. Palai, S. Sharma, " Structural, Dielectric and Electrical Properties of Lead Cadmium Tungstate Ceramics", *Materials Science and Engineering*, B, Vol.77(3), pp. 235–240, 2000.
- [18] K. A. Jassim and H. H. Sahi, Partial replacement of lanthanum (La) and its effect on the insulating properties of the superconducting system - Bi<sub>2</sub>Sr<sub>2</sub>Ca<sub>2</sub>Cu<sub>3</sub>, (BSCCO) (δ + xLa<sub>x</sub>O<sub>10</sub>) *Karbala University Scientific Journal*, Volume 15, Second Issue, 2017.
- [19] G. Korotcenkov, " Handbook of Gas Sensor Materials", Springer LLC, New York (2013).
- [20] Muthafar F. Jamil Al-Hilli, Structural and dielectric properties of Zr doped BaTiO<sub>3</sub> synthesized by microwave assisted chemical route, vol.59, no.1A, (2018).
- [21] Fwad Tariq, Design and Construction of low-Pressure D.C.-Sputtering plasma system for preparing Gas Sensors, Ph.D. thesis, University of Baghdad, 2013.
- [22] Sarmed Salih Al-Awadi, Amer A Ramadhan, Fuad T Ibrahim, Ali K Abbood, ,Optical and Structural Properties of Titanium Dioxide Papered by DC Magneto-Sputtering as a NO<sub>2</sub> Gas Sensor, *Iraqi journal of science*, vol.61, no. 10, (2020).